Supporting Information (SI)

Synthesis and Enantioseparation of Proline-Derived Helical Polyacetylenes as Chiral Stationary Phases for HPLC

Ge Shi[a,#], Xiao Dai[b,#], Yue Zhou[a], Jie Zhang[a], Jun Shen[b,], Xinhua Wan[a,]**

[a]Beijing National Laboratory for Molecular Sciences, Key Laboratory of Polymer Chemistry and Physics of Ministry of Education, College of Chemistry and Molecular Engineering, Peking University, Beijing 100871, China.

[b]Polymer Materials Research Center, Key Laboratory of Superlight Materials and Surface Technology, Ministry of Education, College of Materials Science and Chemical Engineering, Harbin Engineering University, Harbin 150001, China

[#] These authors contribute equally to this work.

* Corresponding authors.

Prof. Xinhua Wan, 86-10-62754187 (Tel), 86-10-62751708 (Fax), Email: xhwan@pku.edu.cn

Prof. Jun Shen, 86-451-82569890 (Tel), Email: shenjun@hrbeu.edu.cn

Table of Contents

1. Experimental Section

Materials. HPLC solvents (tetrahydrofuran, *N*,*N*-Dimethylformamide, n-hexane and isoproponal), anhydrous solvents (dichloromethane and methanol) and common organic solvents were purchased from Xilong Scientific, Concord Technolggy, 3A Chemicals and Tongguang Chem. N-(*tert*-butoxycarbonyl)-(*S*)-prolinal was purchased from OuheChem. Isocyanate reagents were purchased from Energy Chemical, HEOWNS, and Shanghai Dibai Biotech. Racemates were purchased from Energy Chemical, Bide Pharmatech Ltd., HEOWNS, Accela, Shanghai Dibai Biotech and Aladdin. $[Rh(nbd)Cl]_2$ was purchased from Alfa Aesar. 4M HCl-dioxane was purchased from Energy Chemical. Dimethyl (1-Diazo-2-oxopropyl) phosphonate was purchased from Accela. K_2CO_3, NaCl and Na_2SO_4 were purchased from Tongguang Chem. Wide-pore silica gel (Daiso gelSP-1000) with a mean particle size of 7 μm and a mean pore-diameter of 100 nm, which was kindly supplied by Daiso Chemical (Osaka, Japan), was silanized using (3-aminopropyl)triethoxysilanein toluene at 80 ^{o}C.

Instrumentation and Analysis.

NMR spectra were recorded on a Bruker ARX 400 instrument at ambient temperature using either $CDCl_3$ or d_8-THF as the solvent and tetramethylsilane as the internal standard (400 MHz for ^{1}H, and 101 MHz for ^{13}C). High-resolution mass spectra were obtained on a Bruker BIFLEX III mass spectrometer. The number-averaged molecular weight (M_n), weight-averaged molecular weight (M_w), and polydistribution index (M_w/M_n) of polymer were estimated on a gel permeation chromatography (GPC) apparatus equipped with a Waters 2410 refractive index detector and a Waters 515 pump. THF was employed as the eluent at a flow rate of 1.0 mL/min at 25 °C. All GPC curves were calibrated against a series of monodispersed polystyrene standards. Thermogravimetric analyses (TGA) were carried out on a TA Instrument Q600 analyzer at a heating rate of 20 ^{o}C/min under a N_2 flow rate of 100 mL/min. Laser Raman spectra were measured on a Thermo Scientific Nicolet NXR FT-Raman Spectrometer. UV−Vis absorption measurements were conducted on a Varian Cary 1E UV−Vis spectrometer. Optical rotations were recorded on a JASCO Model P-1030 digital polarimeter. Circular dichroism (CD) spectra were

performed on a JASCO J-810 spectrometer. The light path length of the quartz cell used was 10 mm. The samples were dissolved in THF and DMF at a concentration of around 1.2×10^{-4} mol/L. Chromatographic experiments were performed using a JASCOPU-2089 chromatograph equipped with UV–Vis (JASCO UV-2070) and circular dichroism (JASCO CD-2095) detectors at room tem-perature. A solution of a racemate (3 mg/mL) was injected into thechromatographic system through an intelligent sampler (JASCO AS-2055). The elemental analysis was performed on Elementar Vario EL CUBE (Germany).

The 3D skeleton of polymeric stationary phase was conducted in the Material Studio software (version 5.0; Accerlys Software Inc.). First, the structures of repeated units were optimized using the geometry optimization of the Forcite module. To build polymer conformation, the dihedral angles of C−C=C−C and C=C−C=C, hereafter named θ and φ, were varied systematically in steps of 10^{o}. The atactic polymers with 50 repeating units were then built up using Polymer Builder in the Material Studio, in which the dihedral angles were constrained to specific degrees. The structures were subjected to energy minimization with Smart Minimizer of the Discover module at first. Atomistic MD simulations were conducted with the Dynamics of Discover module with a NVT ensemble at 298 K. The total simulation time is 5.0 ps, and time step is 1 fs. The lowest energy 50-mer was only remained the middle 10 repeating units for the docking study.[1]

The docking study was carried out with AutoDock 4.2. The polymeric 10-units were loaded Gasteiger charges and calculated the affinity maps on a 70 × 70 × 70 (0.375 Å spaced) rectangular box centered on the target structure. The molecular docking of enantiomers was subjected to a total of 50 Lamarckian Genetic Algorithm runs. Set the population size and the number of energy evaluations to 150 and 2.5 million, respectively. The value of the initial coordinate for the center of the ligand, ligand rigid-body orientation, and relative dihedral angles were randomized each run. All conformations were then clustered to RMSD of 2.0, and ranked according to the relative free energy of binding (FEB). The average energy of the best cluster with the lowest docking energy result was chosen as the model for mechanism studies.[2]

Synthesis procedures.

(*S*)-*N*-(*tert*-Butoxycarbonyl)-2-ethynyl pyrrolidine (**mBoc**). Under N_2 atmosphere, the mixture of K_2CO_3 (200 mmol, 28 g) and N-(*tert*-butoxycarbonyl)-(*S*)-prolinal (100 mmol, 20 g) was added

anhydrous methanol (100 mL) at 0 °C. The 35 mL dimethyl (1-diazo-2-oxopropyl)phosphonate (130 mmol, 25 g) in methanol solution was added dropwise by syringe. After stirring for 24 h, the mixture was diluted with petroleum ether-ethyl acetate mixture (200 mL) and filtered. The filter residue was washed with ethyl acetate. The combined eluted solution was concentrated under vacuum and purified by flash chromatography with ethyl acetate-petroleum ether mixtures as the eluent to yield 17.6 g of colorless liquid. Yield: 90%. ^{1}H NMR (400 MHz, $CDCl_3$, δ, ppm): 4.62 - 4.32 (d, 1H, NC*H*), 3.56 – 3.18 (d, 2H, NCH_2), 2.29-2.17 (m, 1H, C≡C*H*), 2.17 – 1.96 (t, 3H, CH_2CH_2), 1.96 – 1.81 (m, H, CH_2), 1.68 – 1.24 (m, 9H, CH_3). ^{13}C NMR (101 MHz, *d*-$CDCl_3$, δ, ppm): 154.0, 84.3, 79.7, 69.5, 47.9, 45.9, 45.4, 33.6, 32.9, 28.4, 24.4, 23.5. HRMS (m/z): $[M+H]^+$ calcd for $C_{11}H_{17}NO_2$, 196.1259; found, 196.1327.

(*S*)-*N*-[(4-Chlorophenyl)carbamoyl]-2-ethynyl pyrrolidine (**m^{4}Cl**). Under the N_2 atmosphere, 4.0 g 2-*(S)*-Acetenyl-*N*-(*tert*-butoxycarbonyl)-pyrrolidine was added 35 mL 4 M HCl-dioxane in 150 mL round-bottom flask. After stirring for 2 h, the solvent was removed under vacuum. The residue was mixed with 40 mL anhydrous dichloromethane and 7 mL triethylamine at 0 °C. 5.0 g 4-chlorophenyl isocynate was soluble in 15 mL anhydrous dichloromethane and added to the solution dropwise. After stirring for 24 h, the solution was washed by water and NaCl aqueous solution. The organic solution was dried by Na_2SO_4 and filtered to remove salt. The crude product was obtained by the removal of solvent under reduced pressure and purified by column chromatography with ethyl acetate-petroleum ether mixtures as the eluent to yield 4.8 g of faint yellow solid. Yield: 92%. ^{1}H NMR (400 MHz, $CDCl_3$, δ, ppm): 7.33 - 7.26 (dt, 2H, Ar*H*), 7.19 - 7.12 (dt, 2H, Ar*H*), 6.67 – 6.54 (m, 1H, N*H*), 4.53 – 4.41 (d, 1H, NC*H*), 3.56 – 3.37 (dt, 2H, NCH_2), 2.43 – 2.36 (m, 1H, C≡C*H*), 2.22 – 2.01 (ddt, 3H, CH_2CH_2), 1.99 – 1.86 (dt, 1H, CH_2). ^{13}C NMR (101 MHz, *d*-$CDCl_3$, δ, ppm): 153.5, 137.7, 128.8, 127.8, 120.8, 83.0, 72.6, 47.7, 46.1, 33.8, 24.1. HRMS (m/z): $[M+H]^+$ calcd for $C_{13}H_{13}ClN_2O$, 249.1186; found, 249.0789.

(*S*)-*N*-[(4-Methylphenyl)carbamoyl]-2-ethynyl pyrrolidine (**m^{4}Me**). Yield: 82%. ^{1}H NMR (400 MHz, $CDCl_3$, δ, ppm): 7.26 - 7.20 (d, 2H, Ar*H*), 7.05 - 6.97 (d, 2H, Ar*H*), 6.54 – 6.43 (m, 1H, N*H*), 4.53 – 4.41 (d, 1H, NC*H*), 3.56 – 3.38 (dt, 2H, NCH_2), 2.40 – 2.35 (m, 1H, C≡C*H*), 2.26 – 2.19 (m, 3H, CH_3), 2.18 – 2.00 (ddt, 3H, CH_2CH_2), 1.96 – 1.85 (dt, 1H, CH_2). ^{13}C NMR (101 MHz, *d*-$CDCl_3$, δ, ppm): 153.9, 136.4, 132.5, 129.4, 119.8, 83.3, 72.3, 47.7, 46.1, 33.8, 24.2, 20.8.

HRMS (m/z): $[M+H]^+$ calcd for $C_{14}H_{16}N_2O$, 229.17326; found, 229.1336.

(S)-*N*-[(3-Chloro-4-methylphenyl)carbamoyl]-2-ethynyl pyrrolidine (**m^{3}Cl^{4}Me**). Yield: 94%. ^{1}H NMR (400 MHz, $CDCl_3$, δ, ppm): 7.55 - 7.46 (m, 1H, Ar*H*), 7.23 - 7.16 (d, 1H, Ar*H*), 7.14 - 7.06 (d, 1H, Ar*H*), 6.71 – 6.56 (m, 1H, N*H*), 4.62 – 4.45 (d, 1H, NC*H*), 3.64 – 3.43 (dt, 2H, NCH_2), 2.49 – 2.42 (m, 1H, C≡C*H*), 2.36 – 2.26 (m, 1H, CH_3), 2.26 – 2.07 (ddt, 3H, CH_2CH_2), 2.03 – 1.92 (dt, 1H, CH_2). ^{13}C NMR (101 MHz, *d*-$CDCl_3$, δ, ppm): 153.5, 137.9, 134.2, 130.8, 120.1, 117.9, 83.1, 72.5, 47.7, 46.1, 33.8, 24.2, 19.3. HRMS (m/z): $[M+H]^+$ calcd for $C_{14}H_{15}ClN_2O$, 263.1342; found, 263.0949.

(*S*)-*N*-[3,5-Dimethylphenyl)carbamoyl]-2-ethynyl pyrrolidine (**m2Me**). Yield: 86%. ^{1}H NMR (400 MHz, $CDCl_3$, δ, ppm): 7.09 - 7.03 (m, 2H, Ar*H*), 6.70 - 6.64 (m, H, Ar*H*), 6.60 – 6.48 (m, 1H, N*H*), 4.60 – 4.47 (d, 1H, NC*H*), 3.61 – 3.45 (dt, 2H, NCH_2), 2.48 – 2.43 (m, 1H, C≡C*H*), 2.31 – 2.25 (m, 6H, CH_3), 2.23 – 2.09 (ddt, 3H, CH_2CH_2), 2.03 – 1.93 (dt, 1H, CH_2). ^{13}C NMR (101 MHz, *d*-$CDCl_3$, δ, ppm): 153.8, 138.8, 138.5, 124.7, 117.3, 83.3, 72.3, 47.7, 46.1, 33.8, 24.2, 21.4. HRMS (m/z): $[M+H]^+$ calcd for $C_{15}H_{18}N_2O$, 243.1889; found, 243.1492.

Polymerization.

Monomer m^{4}Cl (7.2 mmol, 1.80 g) and THF (16.5 mL) were added to a dry ampule. After three freeze-pump-thaw cycles, to the ampule was added a solution of $[Rh(nbd)Cl]_2$ (66 mg, 0.143 mmol) and TEA (1.5 mL) in THF (2.0 mL). The concentrations of monomer and the rhodium catalyst were 0.36 and 0.0072 M, respectively. The color of the reaction mixture turned dark red within 1 h. After stirring for 24 h at 30^{o}C, the resulting polymer was precipitated into a large amount of methanol and collected by filtration and washed by methanol. After drying under vacuum at room temperature for 24 h, 1.65 g of paint yellow solids p^{4}Cl were obtained. Yield: 92%. The other polymers were with the same synthetic procedure as p^{4}Cl. All the polymers showed good solubility in THF and slight solubility in DMF.

Preparation of chiral stationary phase.

All these nine polymers were dissolved in THF, then coated on aminopropyl silanized silica gel according to previous method[3]. The silica gels coated with polymers were packed in a stainless-steel tube (25 × 0.20 cm i.d.) by a slurry technique. The plate numbers of the packed columns were 1300–2300 for benzene using a hexane/2-propanol (90/10, v/v) mixture as the eluent at a

flow rate of 0.1 mL/min. 1,3,5-Tri-*t*-butylbenzene was used as a non-retained compound to estimate the dead time (t_0). The rention time of enantiomers is t_1 and t_2. The retention factor k_1 = $(t_1 - t_0) / t_0$, the separation factor $\alpha = (t_2 - t_0) / (t_1 - t_0)$.

Table S1. Elemental analysis of nine polymers.

Polymers	Calculated (%) [a]			Found (%)		
	C	H	N	C	H	N
p^{4}Cl	62.78	5.27	11.26	62.71	5.34	11.21
p^{4}Me	73.66	7.06	12.27	73.58	7.21	12.19
p^{3}Cl^{4}Me	64.00	5.75	10.66	63.91	5.85	10.56
p2Me	74.35	7.49	11.56	74.27	7.57	11.51

[a] Estimated based on a repeating unit.

2. ^{1}H/^{13}C NMR and FTMS Spectra of Important Compounds and Polymers

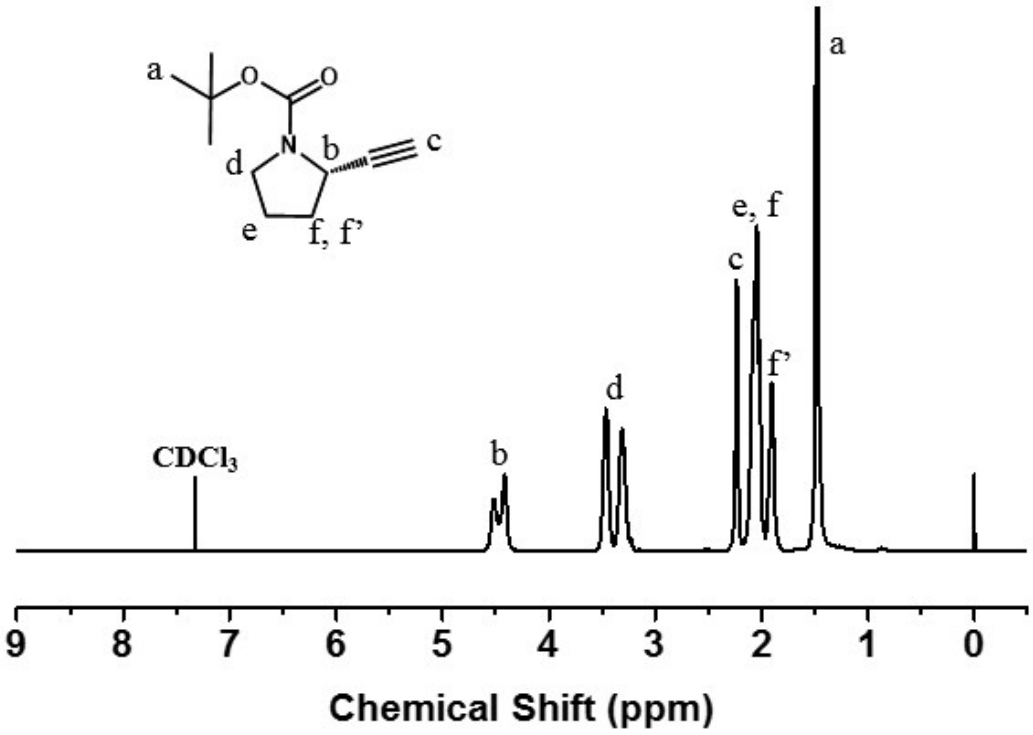

Figure S1. ^{1}H NMR spectrum of mBoc measured in $CDCl_3$ at room temperature.

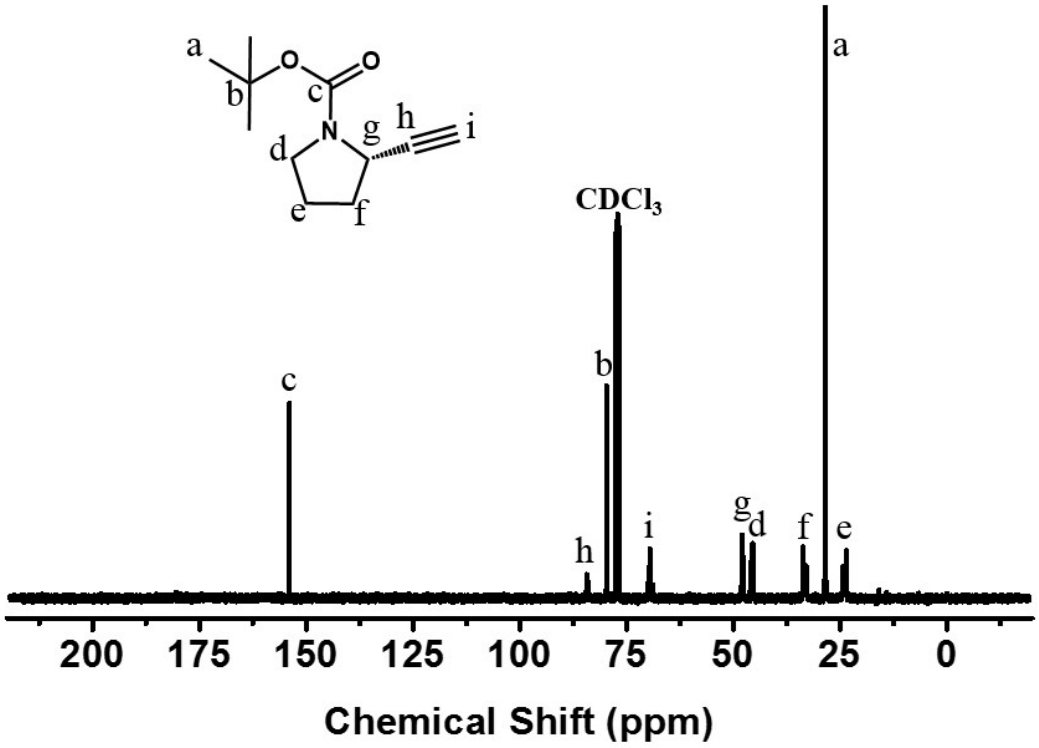

Figure S2. ^{13}C NMR spectrum of mBoc measured in $CDCl_3$ at room temperature.

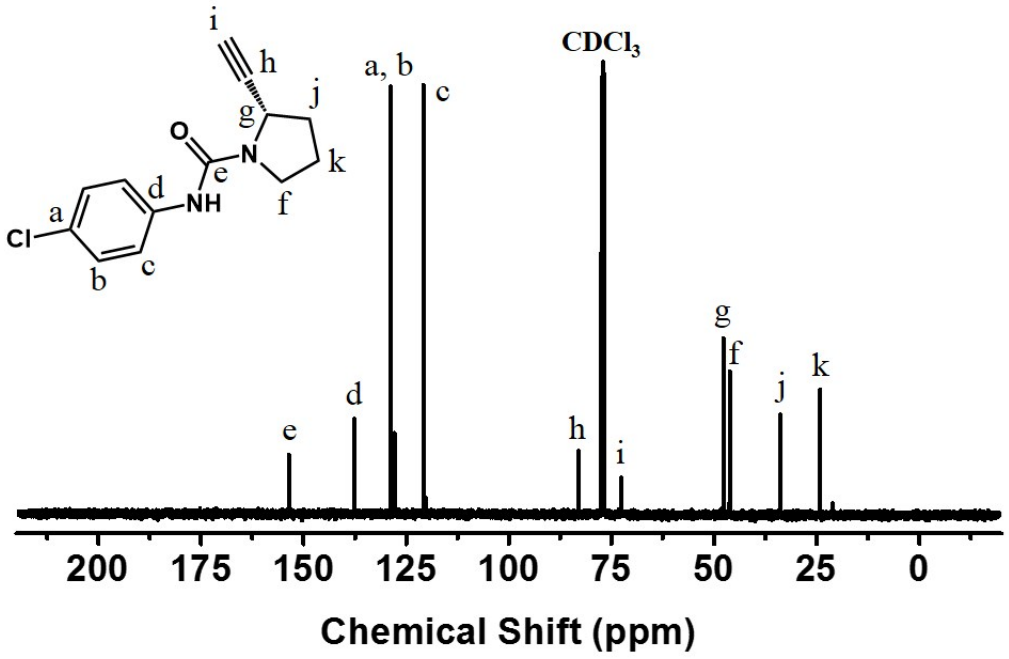

Figure S3. ^{13}C NMR spectrum of m^4Cl measured in $CDCl_3$ at room temperature.

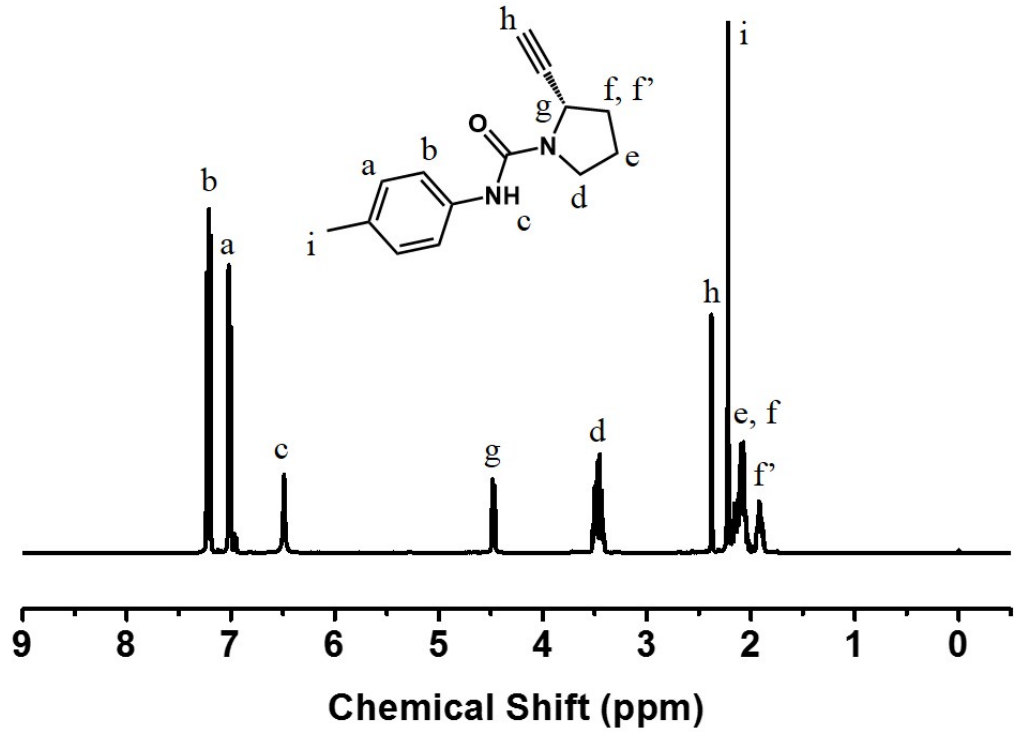

Figure S4. ^{1}H NMR spectrum of m^{4}Me measured in $CDCl_3$ at room temperature.

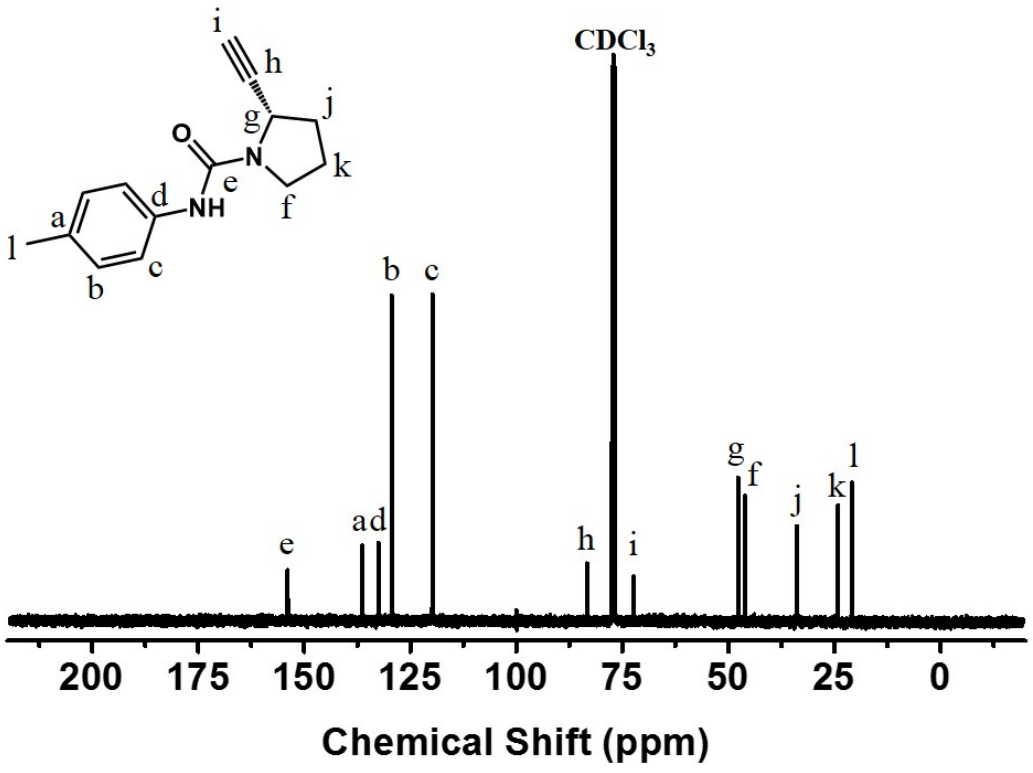

Figure S5. ^{13}C NMR spectrum of m^{4}Me measured in $CDCl_3$ at room temperature.

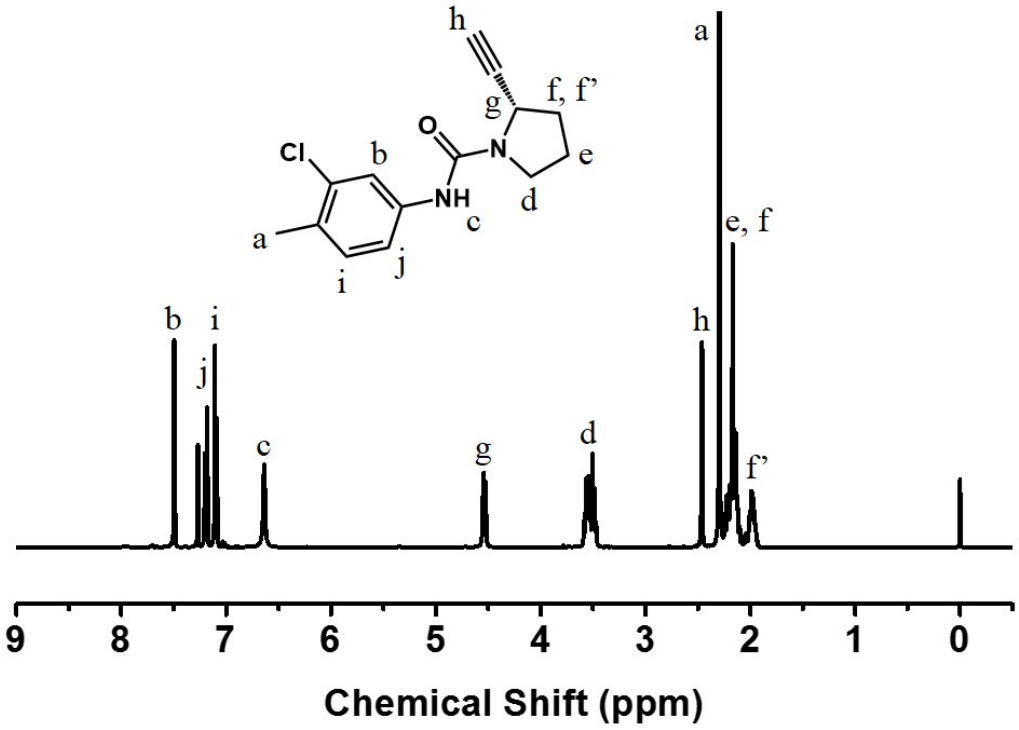

Figure S6. ^{1}H NMR spectrum of m^{3}Cl^{4}Me measured in $CDCl_3$ at room temperature.

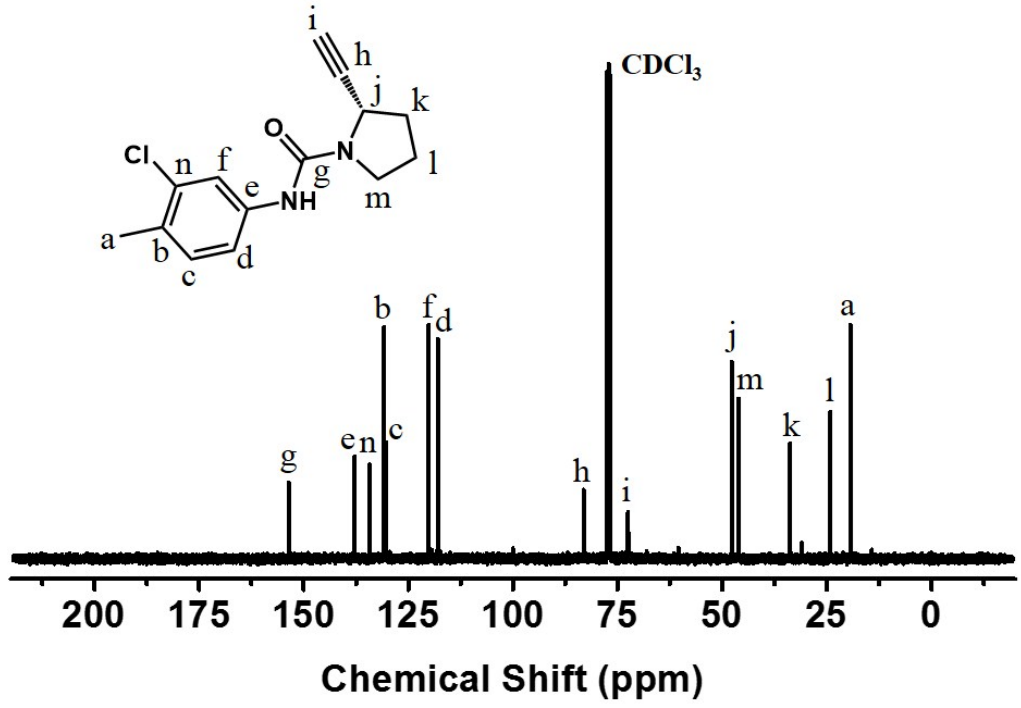

Figure S7. ^{13}C NMR spectrum of m^{3}Cl^{4}Me measured in $CDCl_3$ at room temperature.

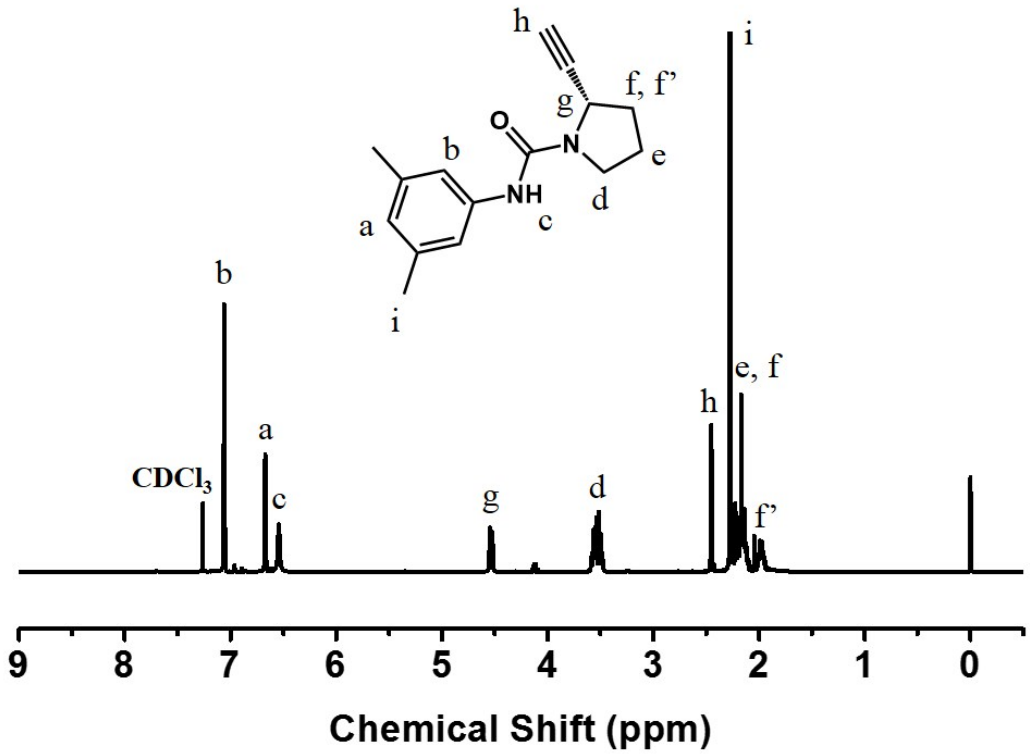

Figure S8. ^{1}H NMR spectrum of m2Me measured in $CDCl_3$ at room temperature.

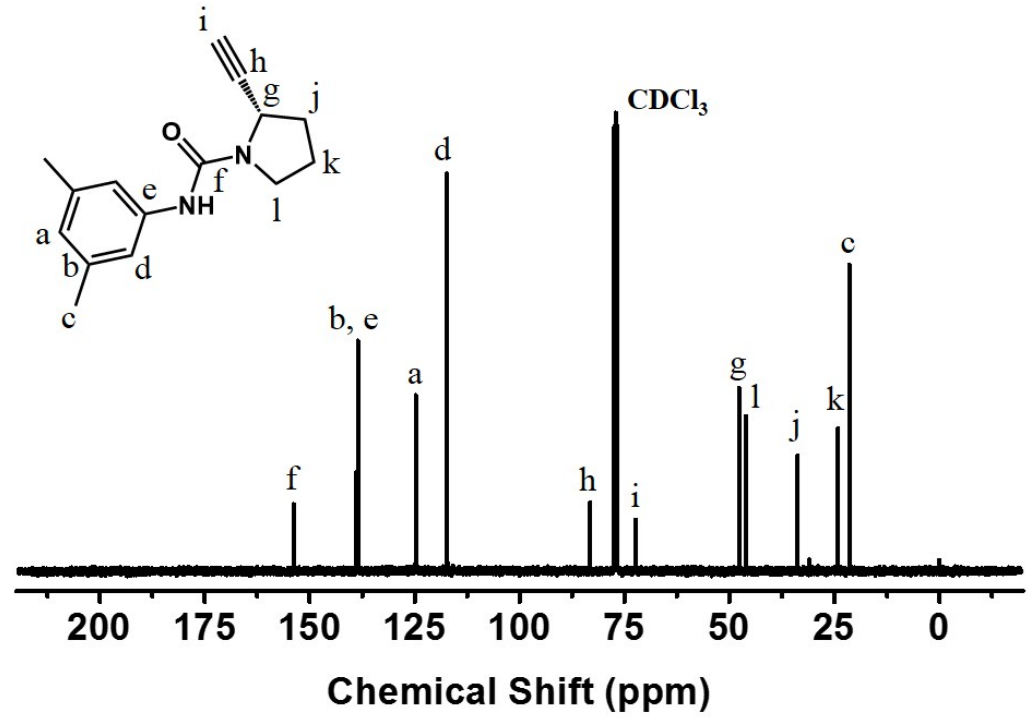

Figure S9. ^{13}C NMR spectrum of m2Me measured in $CDCl_3$ at room temperature.

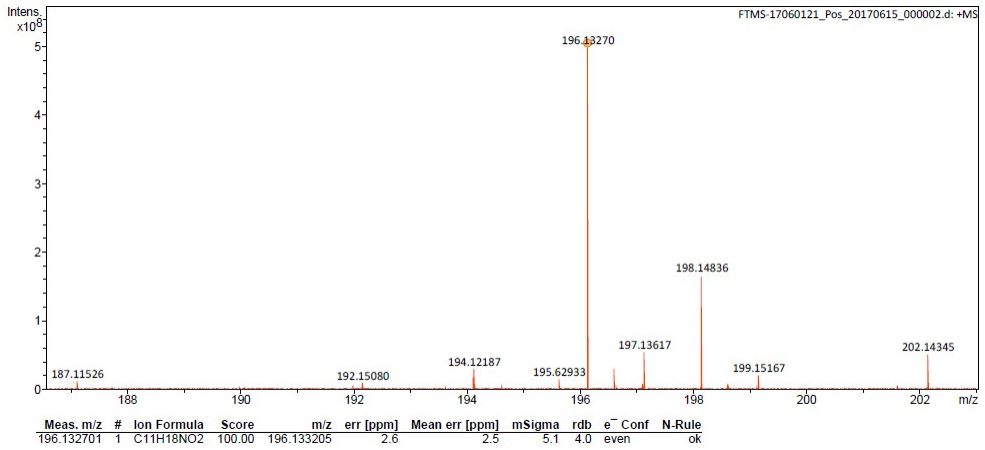

Meas. m/z	#	Ion Formula	Score	m/z	err [ppm]	Mean err [ppm]	mSigma	rdb	e⁻ Conf	N-Rule
196.132701	1	C11H18NO2	100.00	196.133205	2.6	2.5	5.1	4.0	even	ok

Figure S10. FTMS spectrum of mBoc.

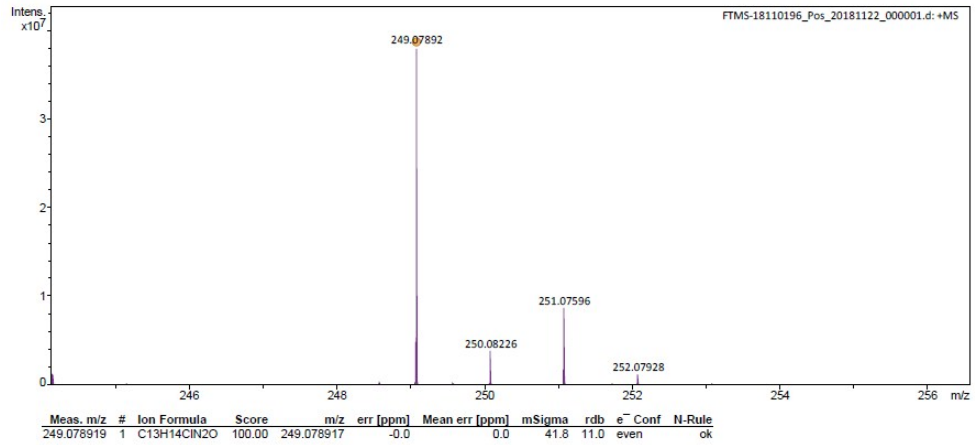

Meas. m/z	#	Ion Formula	Score	m/z	err [ppm]	Mean err [ppm]	mSigma	rdb	e⁻ Conf	N-Rule
249.078919	1	C13H14ClN2O	100.00	249.078917	-0.0	0.0	41.8	11.0	even	ok

Figure S11. FTMS spectrum of m^{4}Cl.

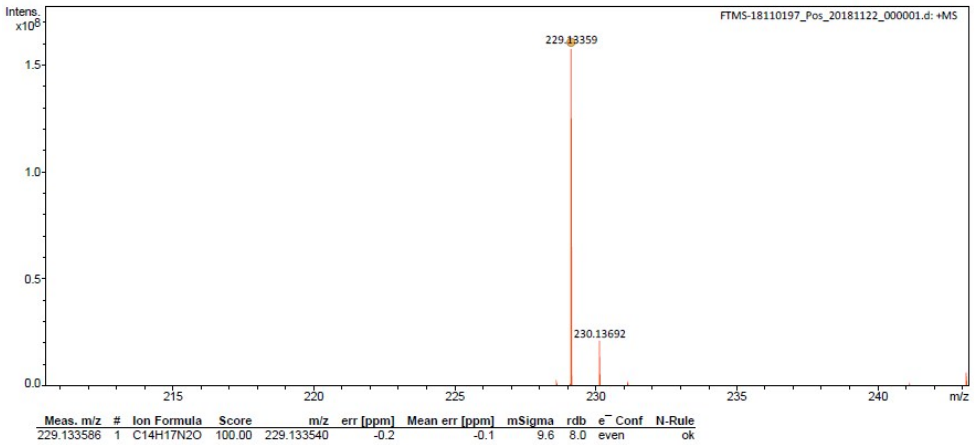

Meas. m/z	#	Ion Formula	Score	m/z	err [ppm]	Mean err [ppm]	mSigma	rdb	e⁻ Conf	N-Rule
229.133586	1	C14H17N2O	100.00	229.133540	-0.2	-0.1	9.6	8.0	even	ok

Figure S12. FTMS spectrum of m^{4}Me.

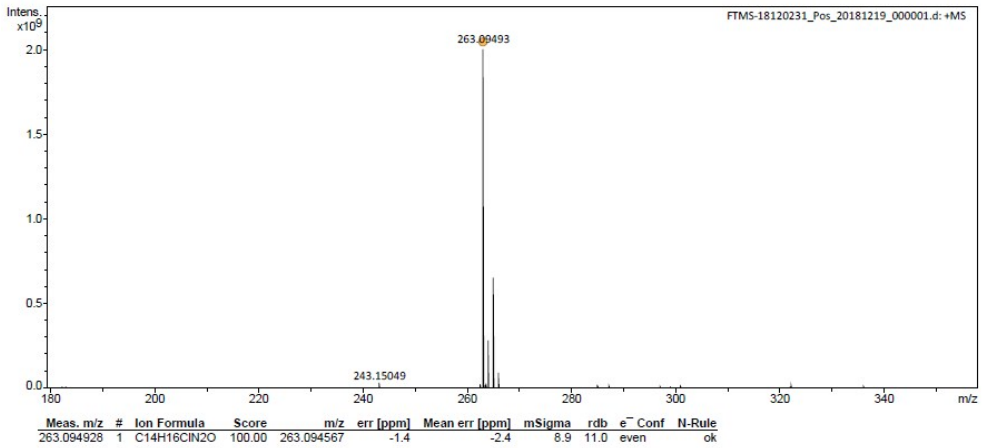

Figure S13. FTMS spectrum of m^3Cl^4Me.

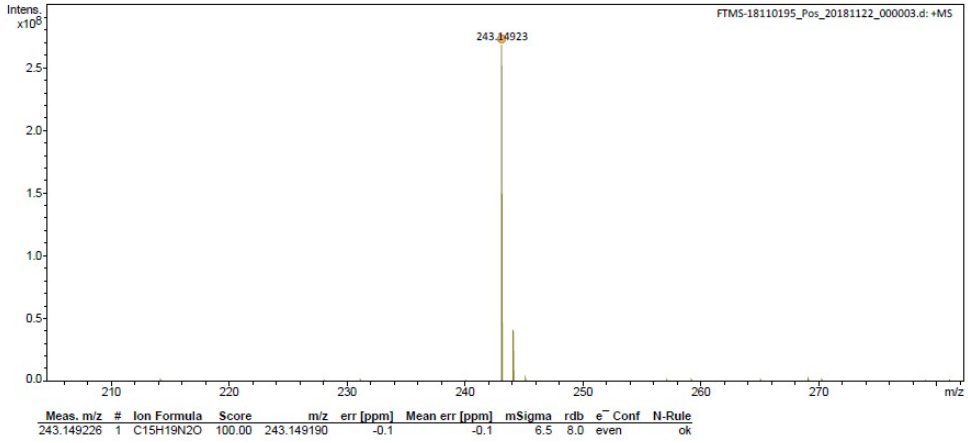

Figure S14. FTMS spectrum of m2Me.

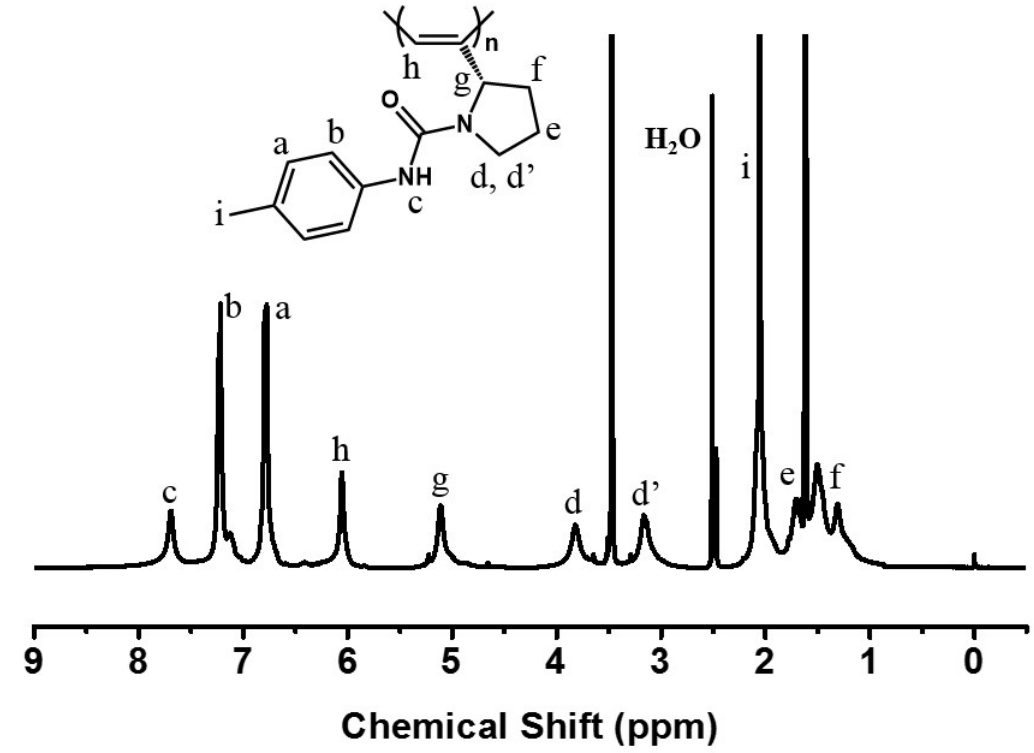

Figure S15. ^{1}H NMR spectrum of p^{4}Me measured in d_8-THF at room temperature.

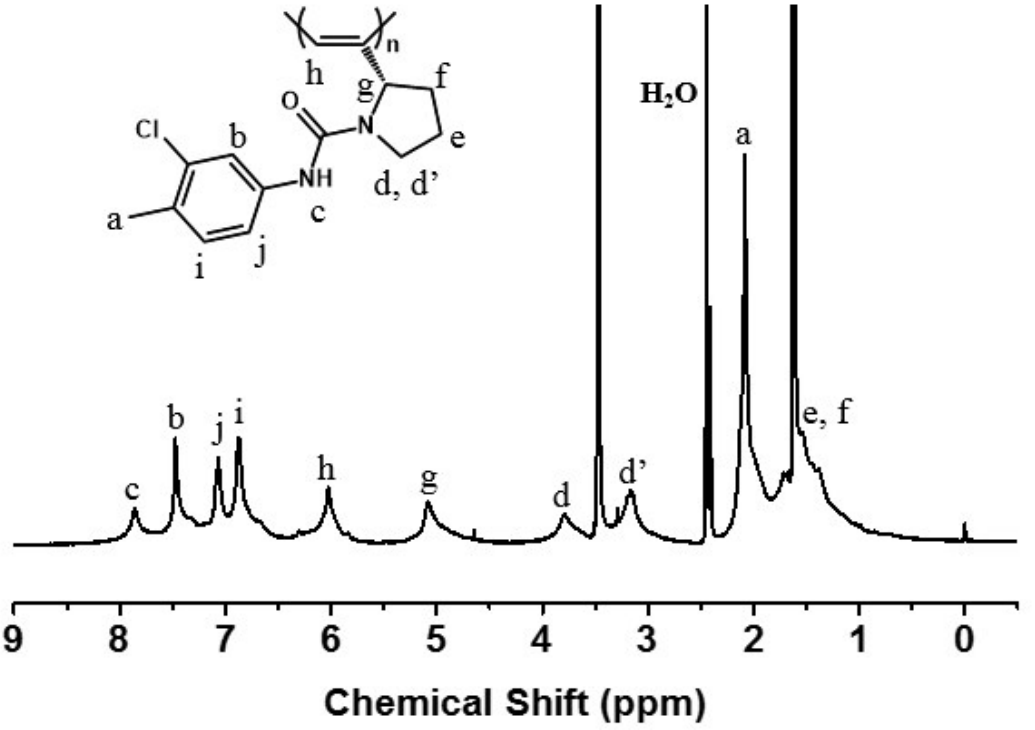

Figure S16. ^{1}H NMR spectrum of p^{3}Cl^{4}Me measured in d_8-THF at room temperature.

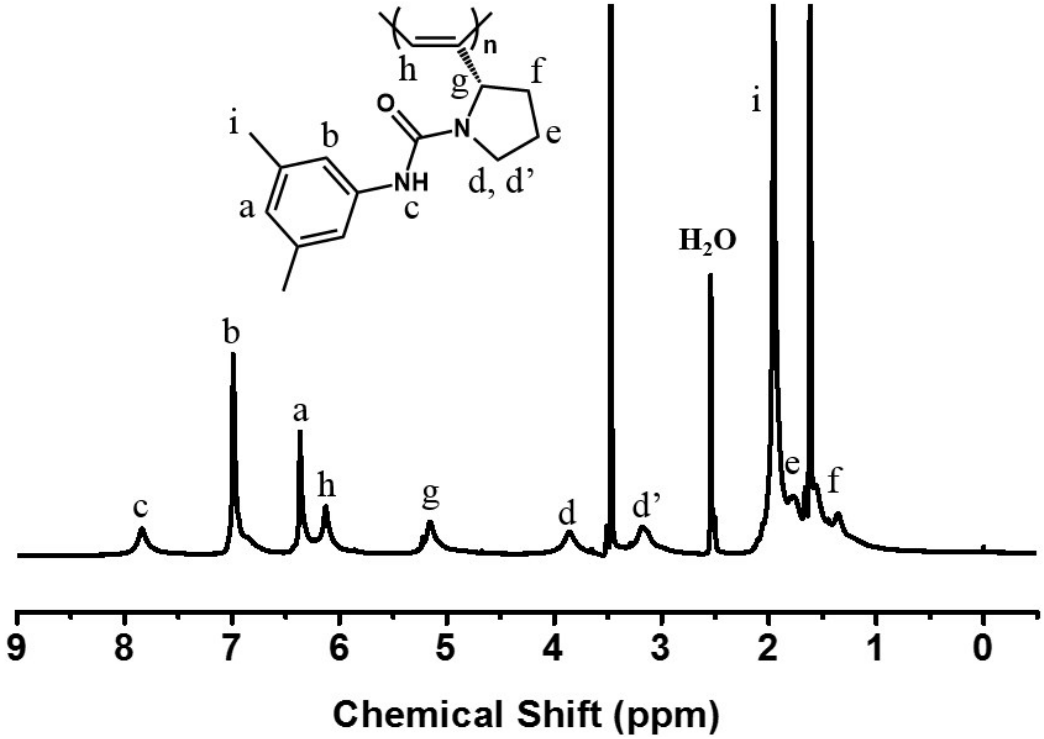

Figure S17. ^{1}H NMR spectrum of p2Me measured in d_8-THF at room temperature.

3. Thermogravimetric Curves of Polymers

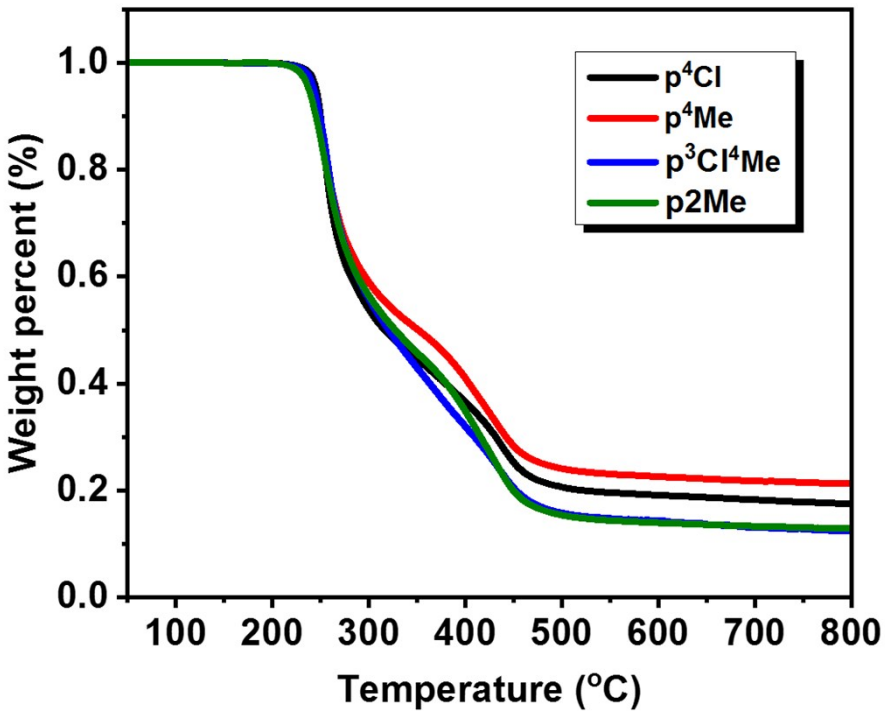

Figure S18. TGA curves of polymers recorded under nitrogen at a heating rate of 20 °C/min.

4. DSC Curves of Polymers

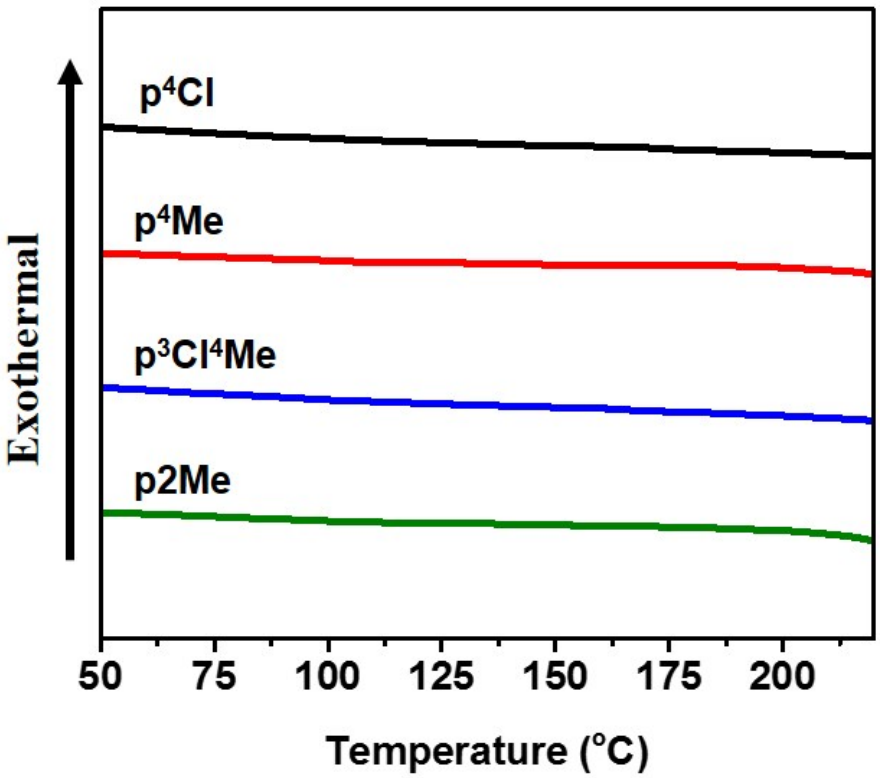

Figure S19. DSC curves of polymers recorded under nitrogen at a heating rate of 10 °C/min.

5. UV-Vis Absorption and CD Spectra

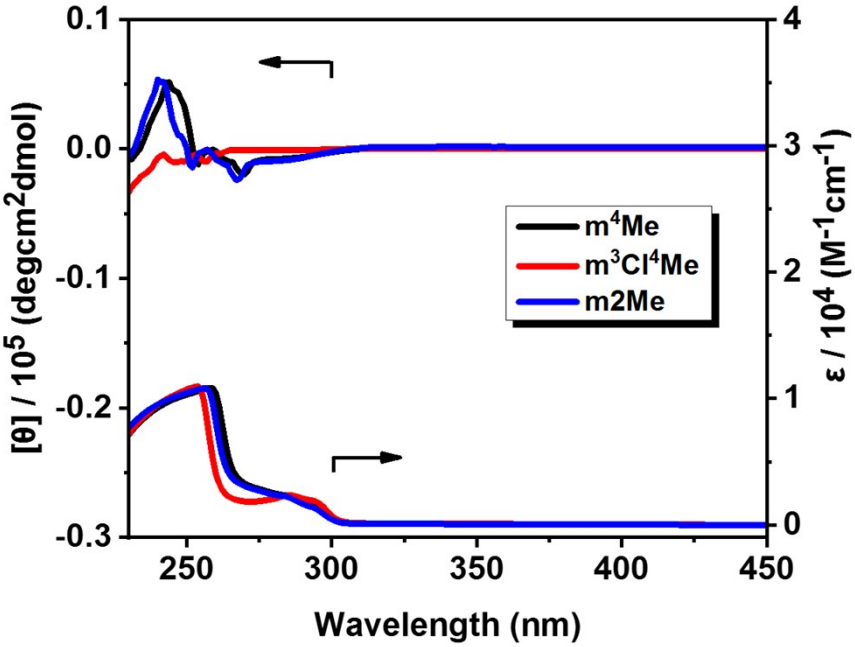

Figure S20. UV-Vis absorption and CD spectra of three monomers in THF at room temperature with a concentration of 1.0 x 10^{-3} mol/L.

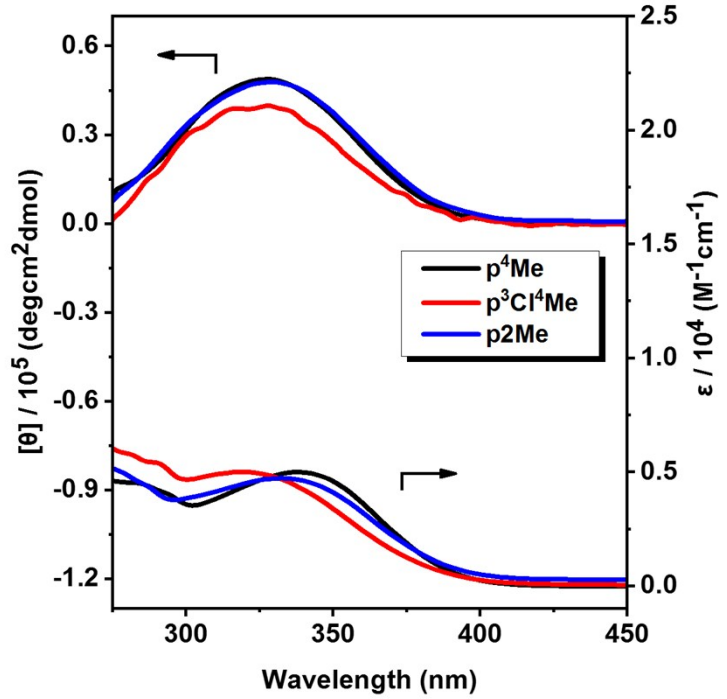

Figure S21. UV-Vis absorption and CD spectra of three polymers in DMF at room temperature with a concentration of 1.2 x 10^{-4} mol/L.

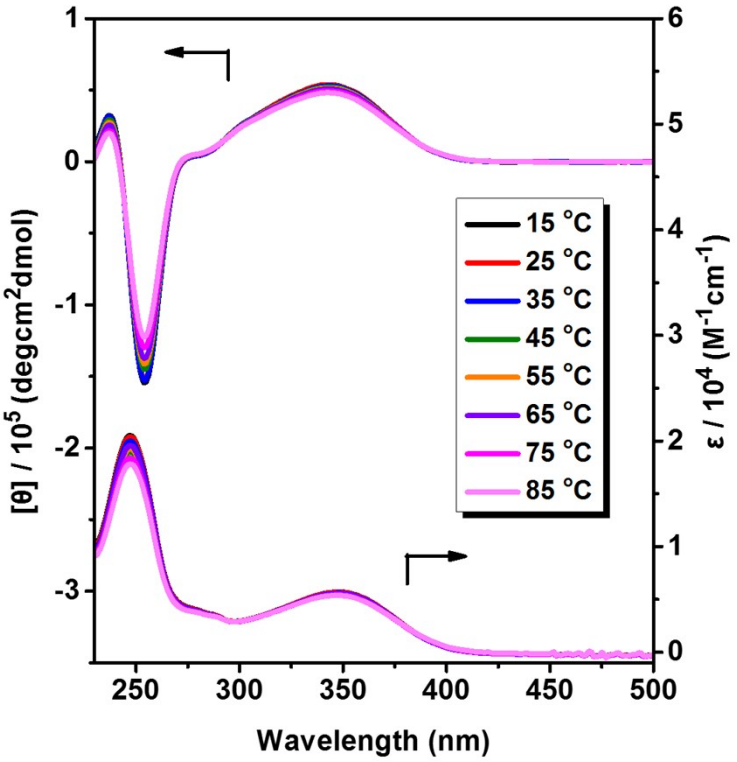

Figure S22. UV-Vis absorption and CD spectra of p2Me in 1,4-dioxane at various temperature with a concentration of 1.2 x 10^{-4} mol/L.

6. HPLC Results

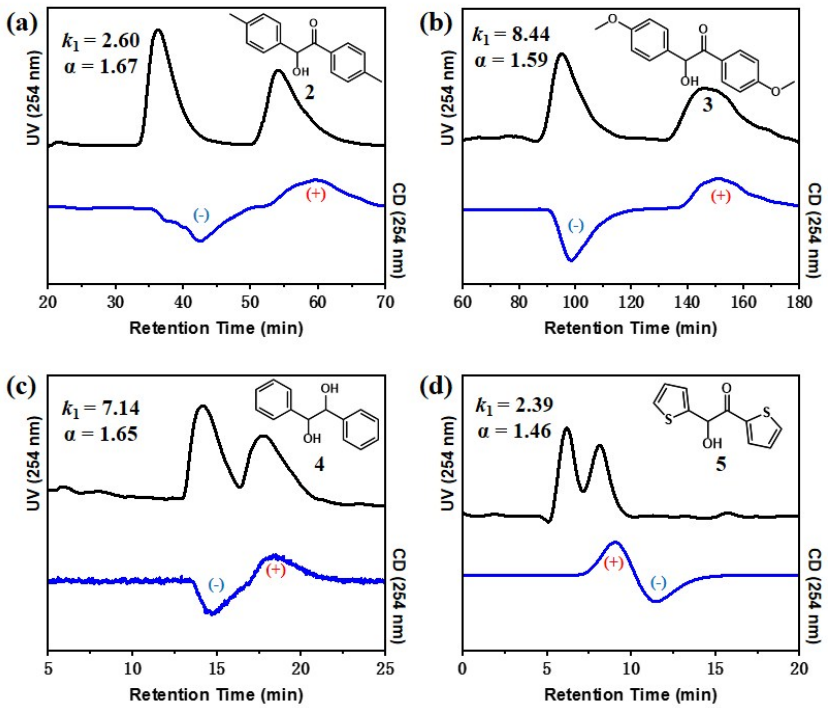

Figure S23. HPLC chromatograms for resolution of (a) **2** on p^{3}Cl^{4}Me-CSP, (b) **3** on p^{3}Cl^{4}Me-CSP, (c) **4** on p^{4}Cl-CSP and (d) **5** on p^{3}Cl^{4}Me-CSP.

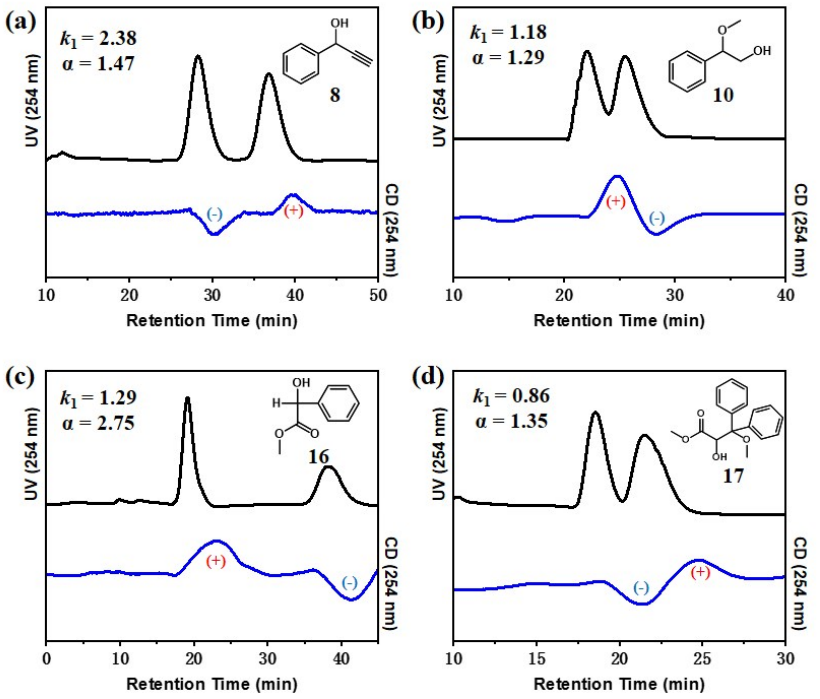

Figure S24. HPLC chromatograms for resolution of (a) **8** on p2Me-CSP, (b) **10** on p^{3}Cl^{4}Me-CSP, (c) **16** on p2Me-CSP and (d) **17** on p^{4}Me-CSP.

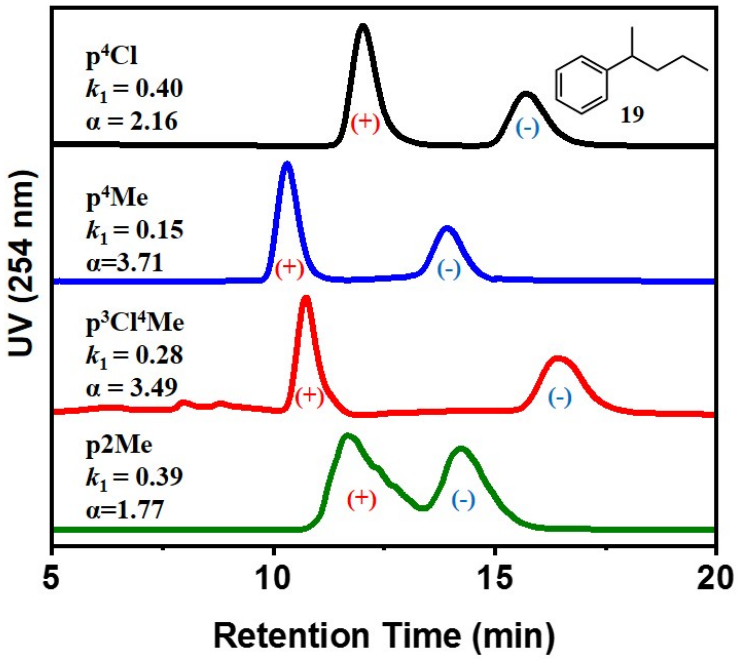

Figure S25. HPLC chromatograms for resolution of **19** on p[4]Cl-CSP, p[4]Me-CSP, p[3]Cl[4]Me-CSP and p2Me-CSP.

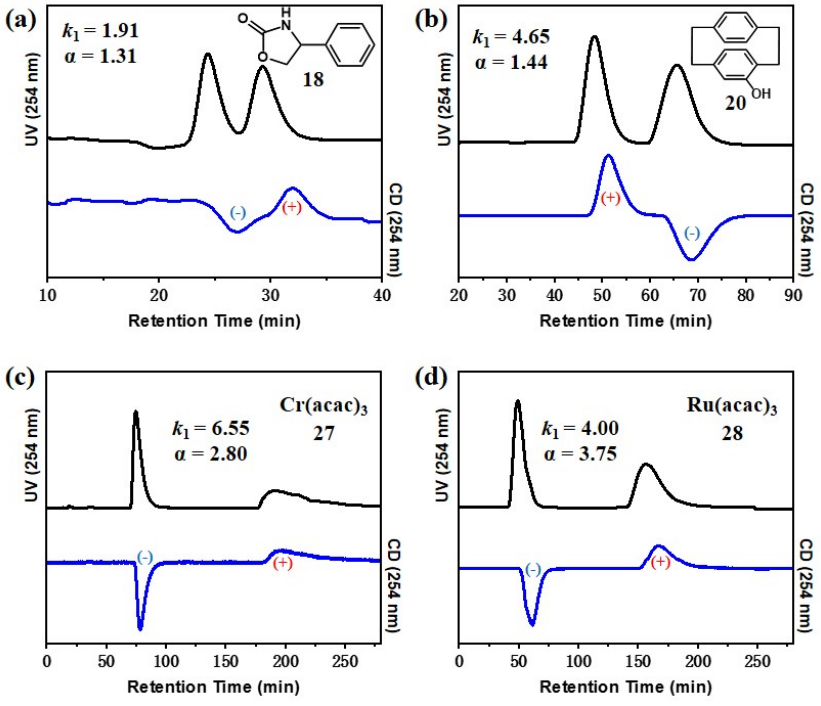

Figure S26. HPLC chromatograms for resolution of (a) **18** on p2Me-CSP, (b) **20** on p[4]Cl-CSP, (c) **27** on p[4]Me-CSP and (d) **28** on p[4]Me-CSP.

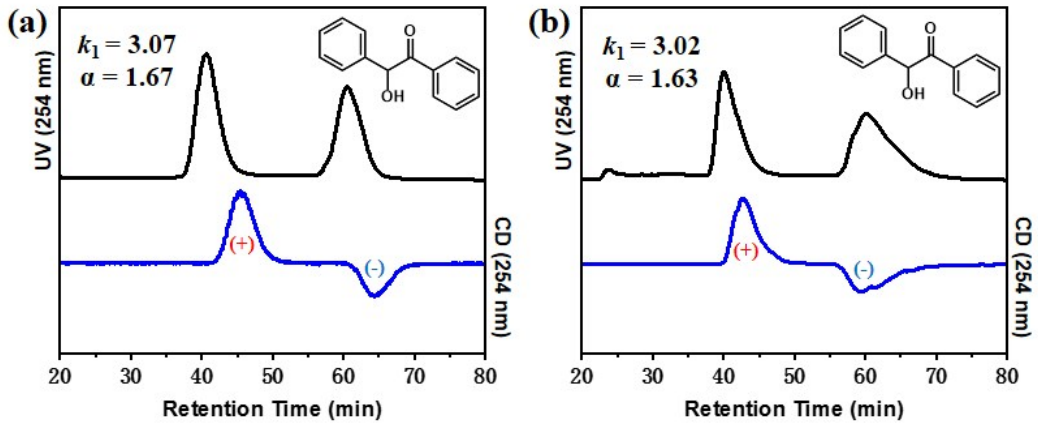

Figure S27. HPLC chromatograms for resolution of **1** on on p^{3}Cl^{4}Me-CSP (a) by immediate test and (b) eight-months-later test.

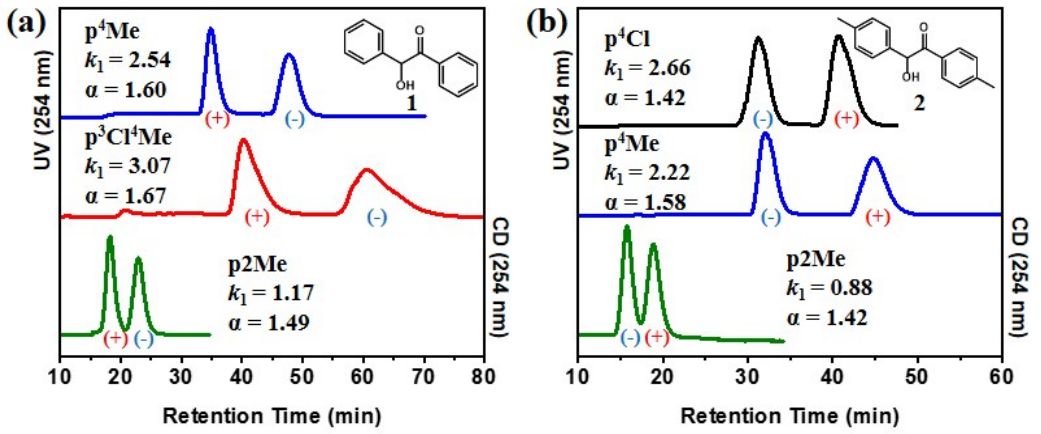

Figure S28. HPLC chromatograms for resolution of (a) **1** and (b) **2** on various CSPs.

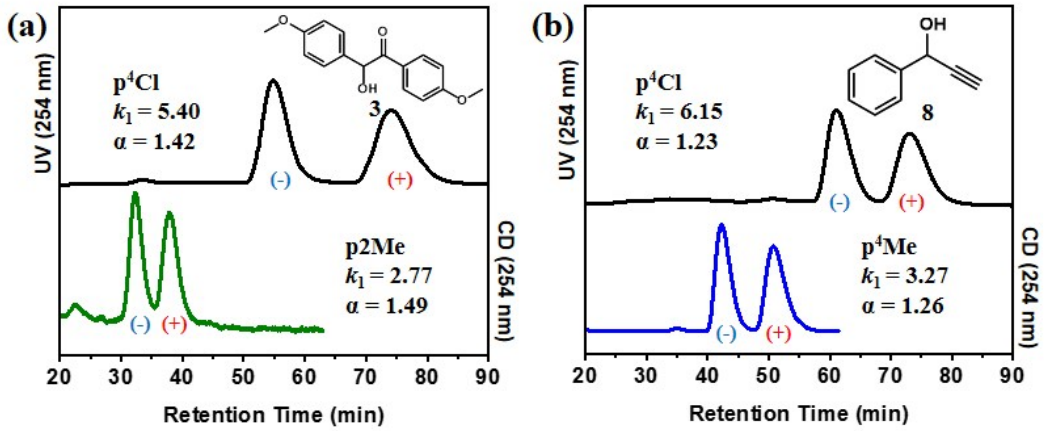

Figure S29. HPLC chromatograms for resolution of (a) **3** and (b) **8** on various CSPs.

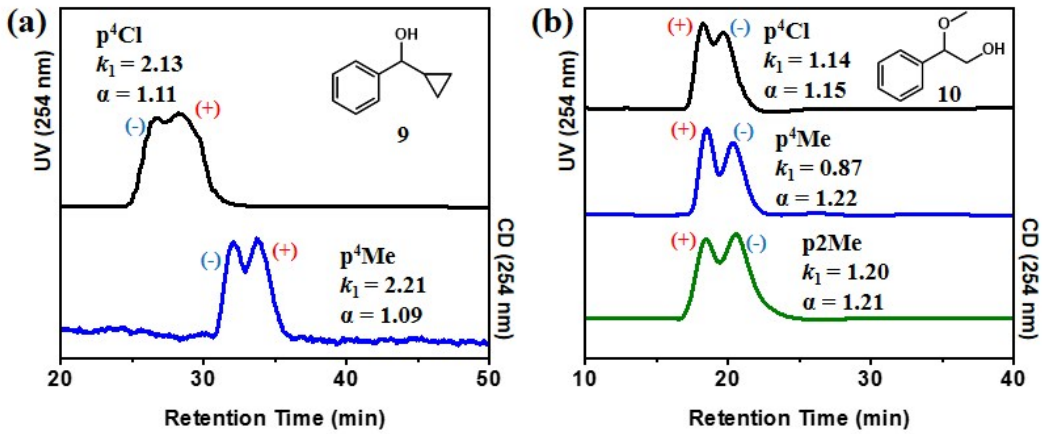

Figure S30. HPLC chromatograms for resolution of (a) **9** and (b) **10** on various CSPs.

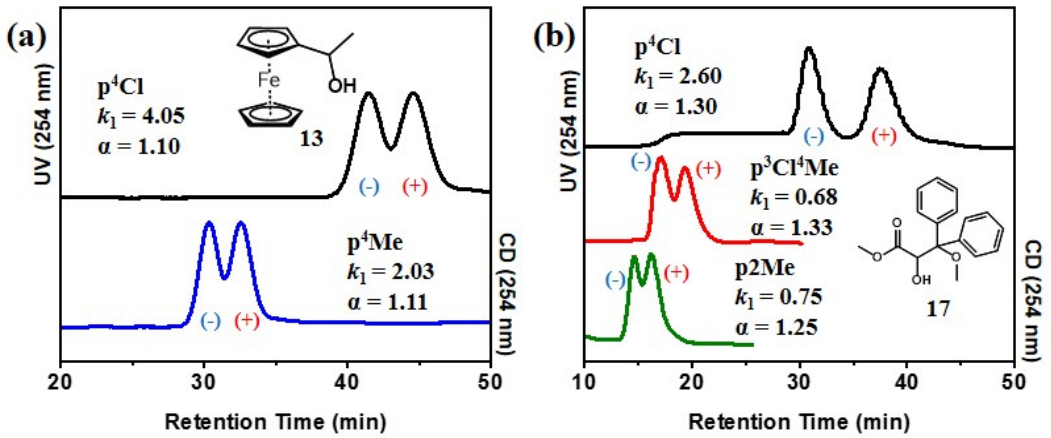

Figure S31. HPLC chromatograms for resolution of (a) **13** and (b) **17** on various CSPs.

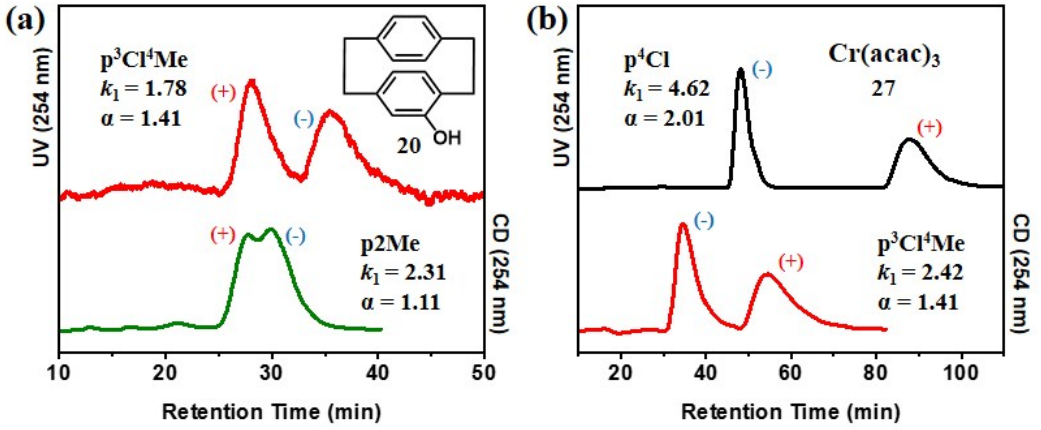

Figure S32. HPLC chromatograms for resolution of (a) **20** and (b) **27** on various CSPs.

7. Computational Simulation

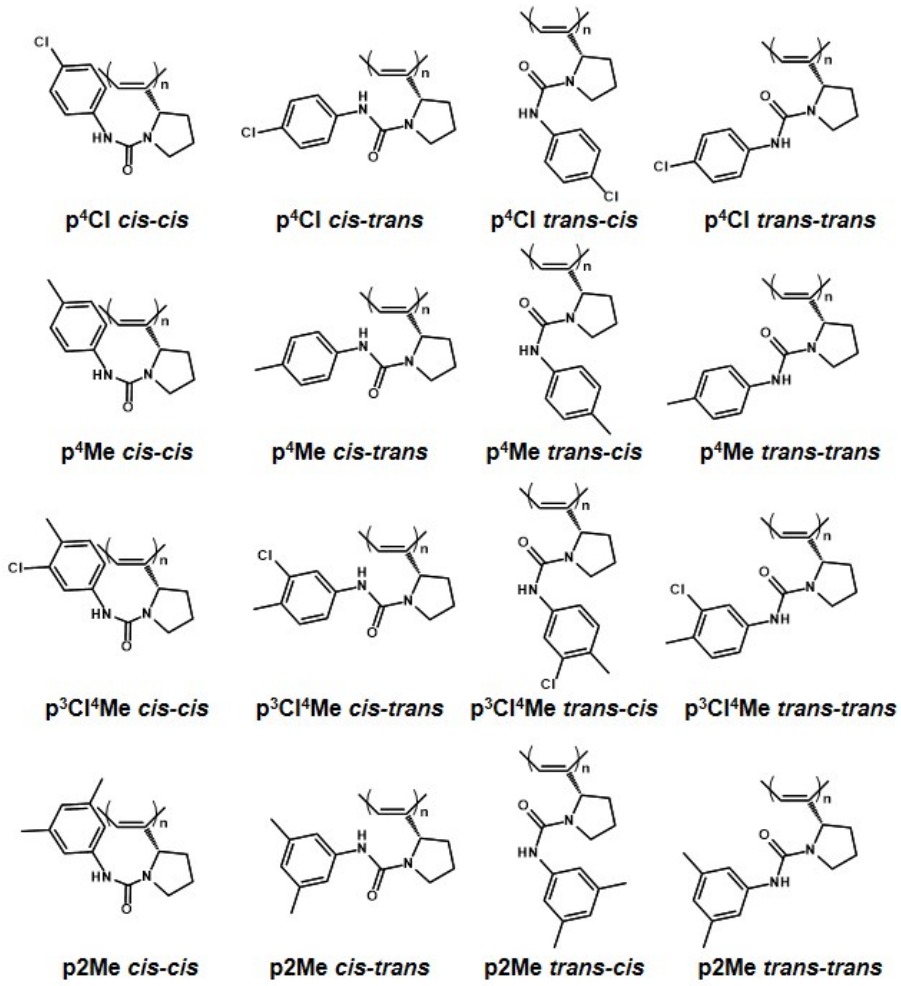

Figure S33. Four conformers of p^4Cl, p^4Me, p^3Cl^4Me and p2Me.

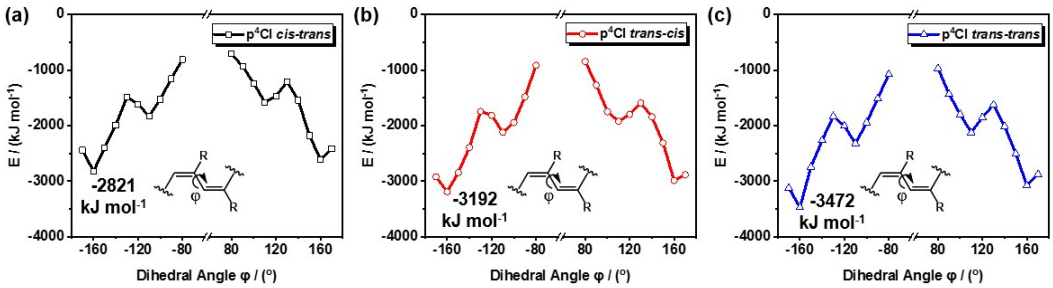

Figure S34. Relationships between the energy and dihedral angle φ at the single bond in the backbones of p^4Cl.

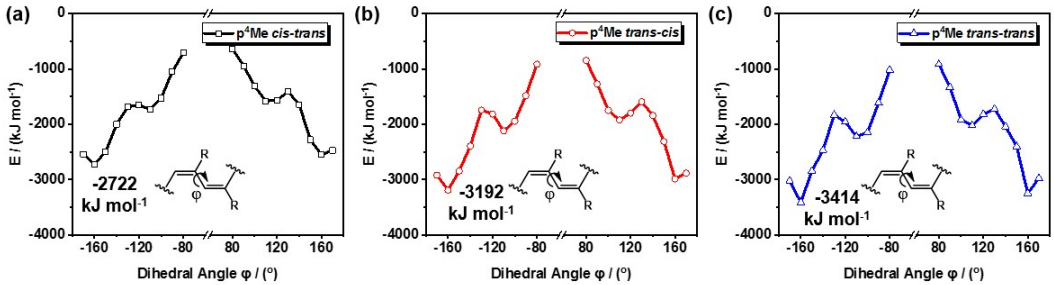

Figure S35. Relationships between the energy and dihedral angle φ at the single bond in the backbones of p^4Me.

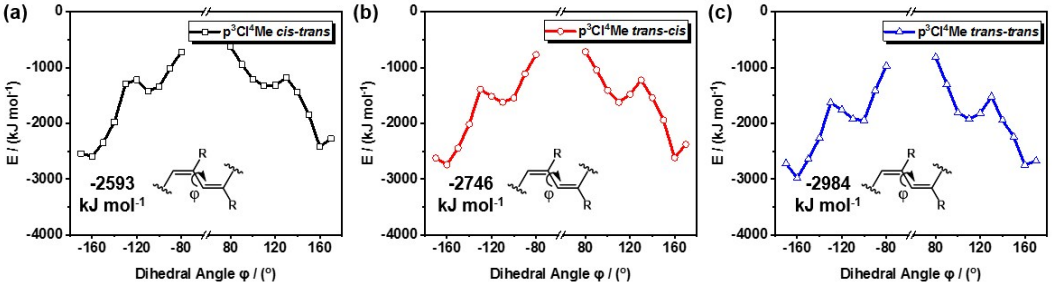

Figure S36. Relationships between the energy and dihedral angle φ at the single bond in the backbones of p^3Cl^4Me.

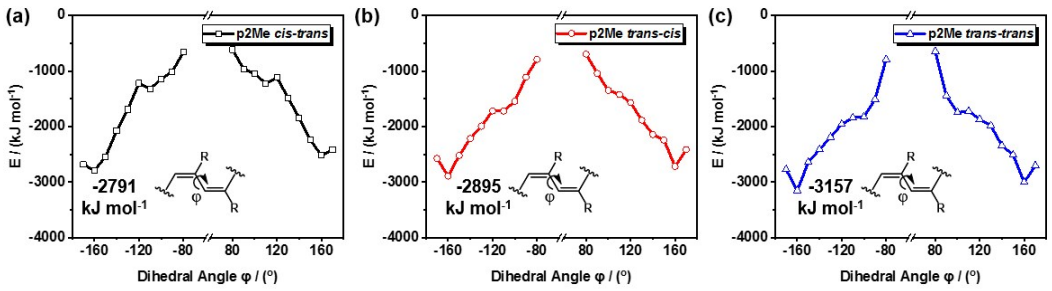

Figure S37. Relationships between the energy and dihedral angle φ at the single bond in the backbones of p2Me.

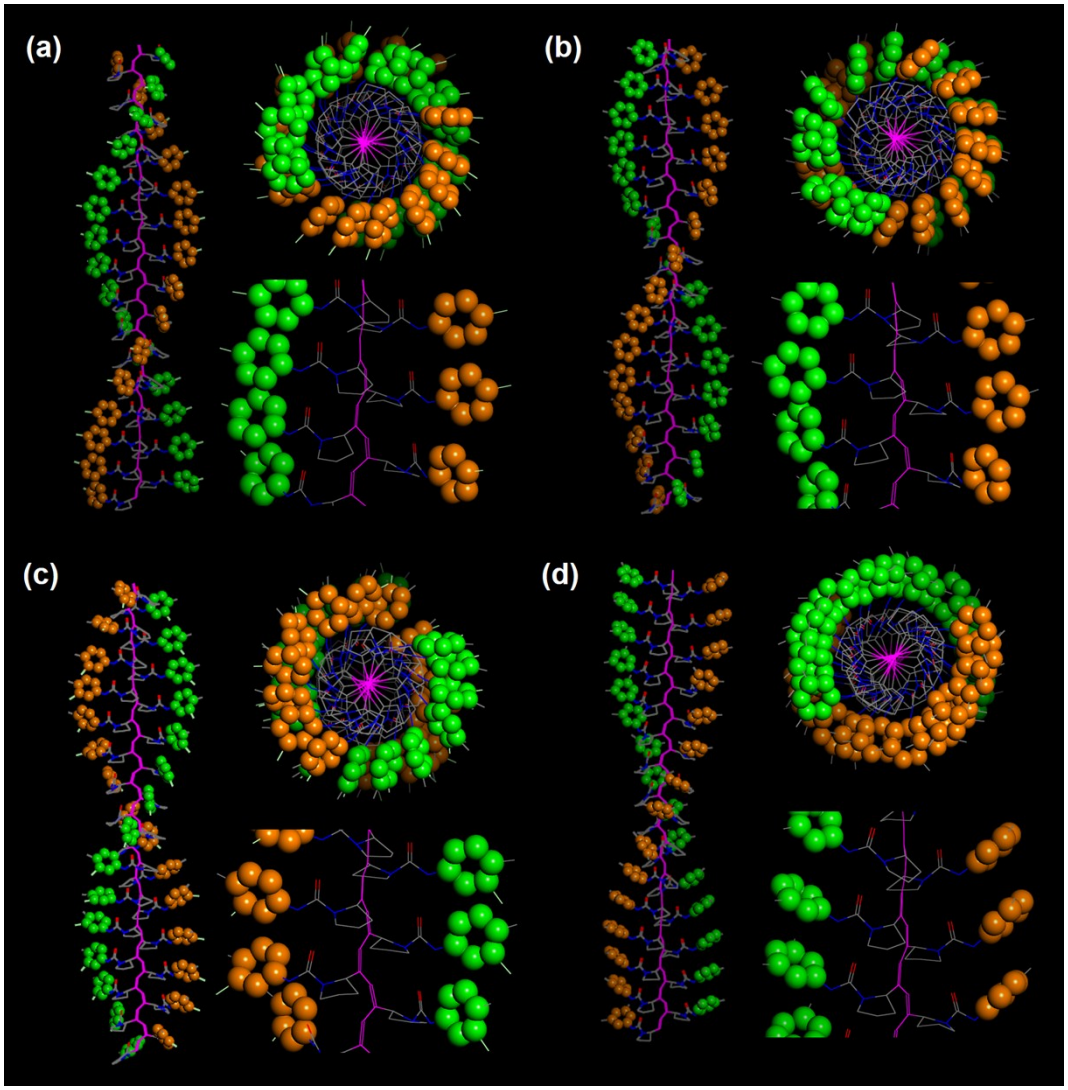

Figure S38. Possible 3D helical structures of *trans-trans* conformers obtained from computational simulations: (a) p^4Cl, (b) p^4Me, (c) p^3Cl^4Me and (d) p2Me.

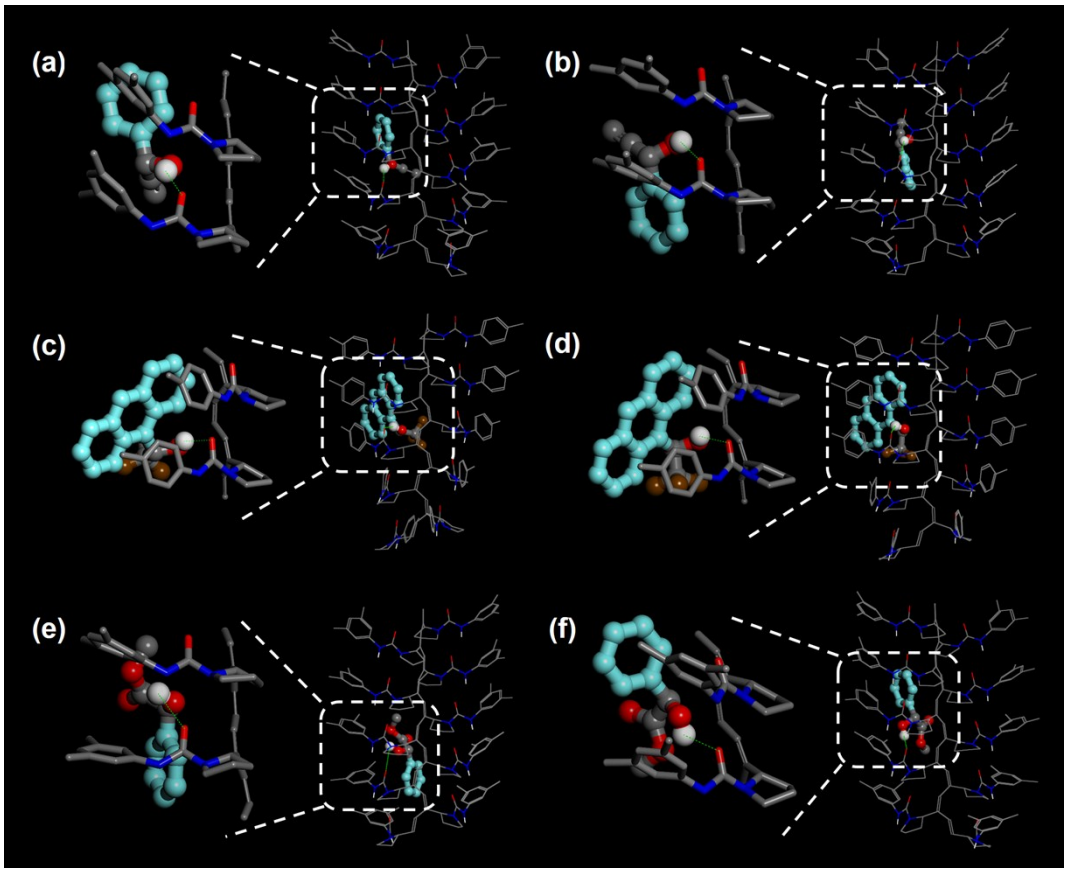

Figure S39. Binding mode of the SA (a) **(+)-8** to p2Me; (b) **(-)-8** to p2Me; (c) **(+)-**15 to p^{4}Me; (d) **(-)-15** to p^{4}Me; (e) **(+)-16** to p2Me; (f) **(-)-16** to p2Me calculated by molecular docking. SA and CS were displayed in ball-stick model and line model, respectively. Atoms were colored as: C (gray), O (red), N (blue), H (white), F (brown); aromatic groups of SA (cyan); HB interactions in green-colored dashed lines.

Table S2. Molecular docking results of enantiomers and CSPs.

CSP	**(+)-8**		**(-)-8**		ΔΔE [d]
	d_{HB} (Å)[a]	$d_{\pi-\pi}$ (Å)[b]	d_{HB} (Å)	$d_{\pi-\pi}$ (Å)[c]	(kJ/mol)
p2Me	2.048	3.739	2.151	-	-1.46
CSP	**(+)-15**		**(-)-15**		ΔΔE [d]
	d_{HB} (Å)	$d_{\pi-\pi}$ (Å)	d_{HB} (Å)	$d_{\pi-\pi}$ (Å)	(kJ/mol)
p^{4}Me	2.298	3.852, 3.821	2.063	3.820, 3.847	+1.72
CSP	**(+)-16**		**(-)-16**		ΔΔE [d]
	d_{HB} (Å)	$d_{\pi-\pi}$ (Å)[c]	d_{HB} (Å)	$d_{\pi-\pi}$ (Å)	(kJ/mol)
p2Me	2.103	-	1.937	3.684	+2.47

[a] The distance between hydrogen atom of SA hydroxyl and oxygen atom of CS urea. [b] The distance between centroid of SA and CS phenyl groups for face-to-face π-π interactions. [c] The distance between

centroid of SA phenyl and carbon atom on CS phenyl for edge-to-face π-π interactions. [d] The difference in free energy of binding, $\Delta\Delta E = \Delta E_{(+)} - \Delta E_{(-)}$.

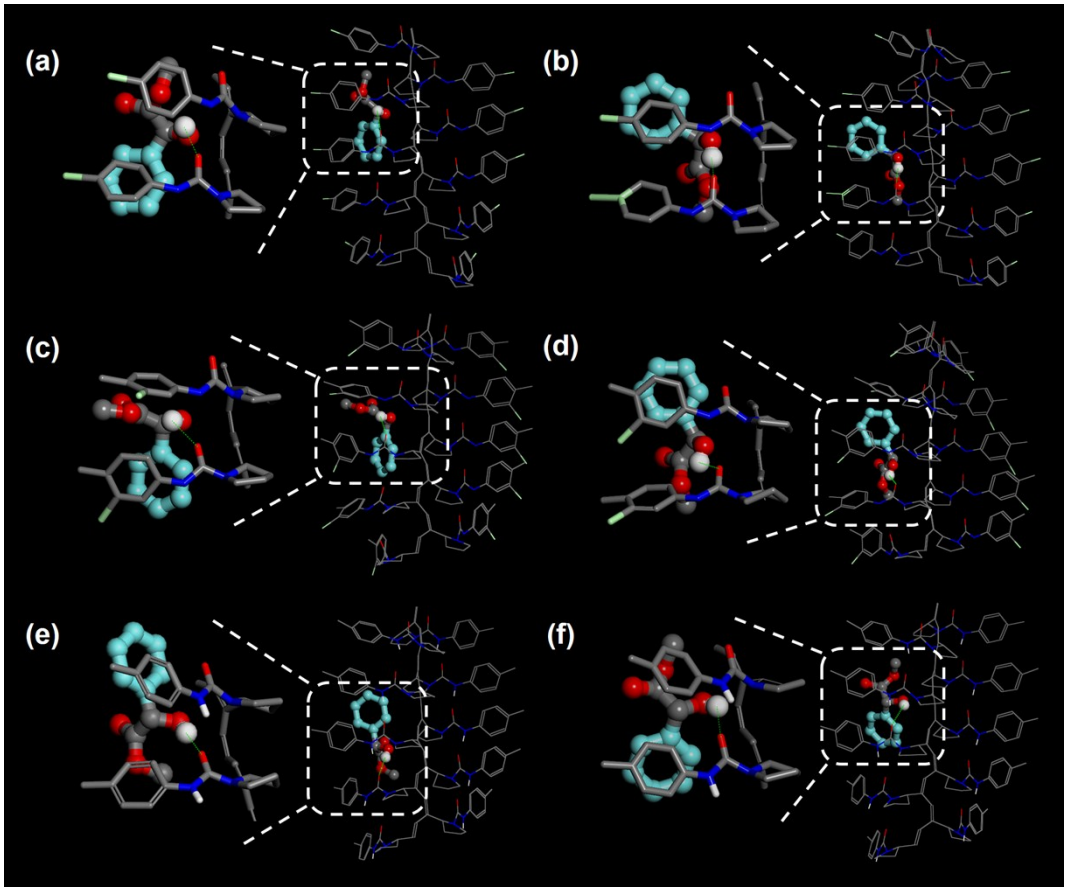

Figure S40. Binding mode of the SA (a) **(+)-16** to p^4Cl; (b) **(-)-16** to p^4Cl; (c) **(+)-**16 to p^3Cl^4Me; (d) **(-)-16** to p^3Cl^4Me; (e) **(+)-16** to p^4Me; (f) **(-)-16** to p^4Me calculated by molecular docking. SA and CS were displayed in ball-stick model and line model, respectively. Atoms were colored as: C (gray), O (red), N (blue), H (white); aromatic groups of SA (cyan); HB interactions in green-colored dashed lines.

Table S3. Molecular docking results of enantiomers and CSPs. [a]

CSP	(+)-16		(-)-16		ΔΔE [c]
	d_{HB} (Å) [a]	$d_{\pi-\pi}$ (Å) [b]	d_{HB} (Å)	$d_{\pi-\pi}$ (Å)	(kJ/mol)
p^4Cl	2.031	3.820	2.068	3.756	-0.08
CSP	**(+)-16**		**(-)-16**		ΔΔE [c]
	d_{HB} (Å)	$d_{\pi-\pi}$ (Å)	d_{HB} (Å)	$d_{\pi-\pi}$ (Å)	(kJ/mol)
p^3Cl^4Me	2.147	3.796	2.116	3.892	+0.21
CSP	**(+)-16**		**(-)-16**		ΔΔE [c]

	d_{HB} (Å)	$d_{\pi-\pi}$ (Å)	d_{HB} (Å)	$d_{\pi-\pi}$ (Å)	(kJ/mol)
p^{4}Me	2.106	3.818	2.138	3.687	+0.12

[a] The distance between hydrogen atom of SA hydroxyl and oxygen atom of CS urea. [b] The distance between centroid of SA and CS phenyl groups for face-to-face π-π interactions. [c] The difference in free energy of binding, $\Delta\Delta E = \Delta E_{(+)} - \Delta E_{(-)}$.

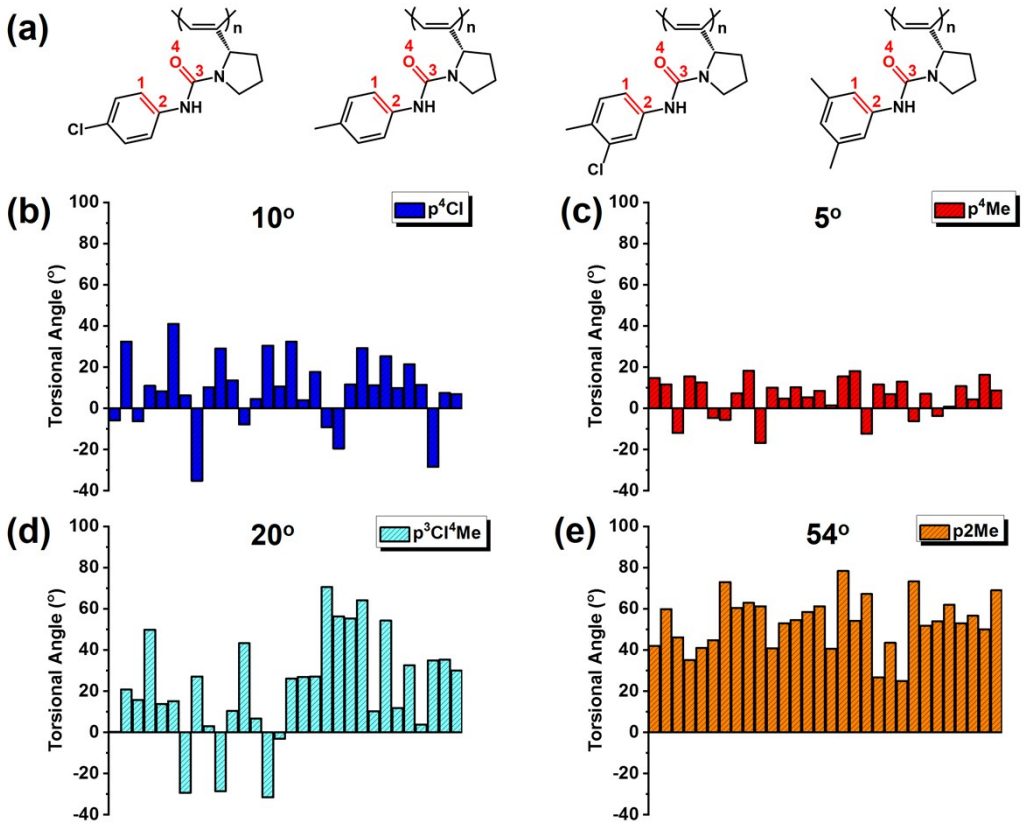

Figure S41. (a) Torsional angle diagrams of four polymers (selected atoms are marked in red); and the simulation results of torsional angle for (b) p^{4}Cl, (c) p^{4}Me, (d) p^{3}Cl^{4}Me, and (e) p2Me.

8. Reference

1. Wang, S.; Feng, X. Y.; Zhao, Z. Z.; Zhang, J.; Wan, X. H. Reversible *Cis-Cisoid* to *Cis-Transoid* Helical Structure Transition in Poly(3,5-disubstituted phenylacetylene)s. *Macomolecules*, **2016**, *49*, 8407-8417.

2. Pisani, L.; Rullo, M.; Catto, M.; Candia, M.; Carrieri, A.; Cellamare, S.; Altomare, C.D. Structure–property Relationship Study of the HPLC Enantioselective Retention of Neuroprotective 7-[(1-alkylpiperidin-3-yl)methoxy]coumarin Derivatives on an Amylose-based Chiral Stationary Phase. *J. Sep. Sci.*, **2018**, *41*, 1376-1384.

3. Shen, J.; Wang, F.; Bi, W. Y.; Liu, B.; Liu, S. Y.; Okamoto, Y. Synthesis of Cellulose Carbamates bearing Regioselective Substituents at 2,3- and 6-positions for Efficient Chromatographic Enantioseparation. *J. Chromatogr. A.*, **2018**, *1572*, 54-61.